An Estimate of Ice Wedge Volume for a High Arctic Polar Desert Environment, Fosheim Peninsula, Ellesmere Island

Claire Bernard-Grand'Maison[1] and Wayne Pollard[2]

[1]Department of Geography, Environment and Geomatics, University of Ottawa, Ottawa, K1N 6N5, Canada
5 [2]Department of Geography, McGill University, Montreal, H3A 0G4, Canada

Correspondence to: Claire Bernard-Grand'Maison (cbern085@uottawa.ca)

Abstract. Quantifying ground-ice volume on a regional scale is necessary to assess the vulnerability of permafrost landscapes to thaw induced disturbance like terrain subsidence and to quantify potential carbon release. Ice wedges (IWs) are a ubiquitous ground-ice landform in the Arctic. Their high spatial variability makes generalizing their potential role in landscape change

10 problematic. IWs form polygonal networks visible on satellite imagery from surface troughs. This study focuses on the estimation of IW ice volume for the Fosheim Peninsula, Ellesmere Island, a continuous permafrost area characterized by polar desert conditions and extensive ground-ice. We perform basic GIS analyses on high resolution satellite imagery to delineate IW troughs and estimate the associated IW ice volume using a 3D subsurface model. We demonstrate two semi-automated IW trough delineation methods with different strengths to increase time-efficiency of this process, done manually in previous

15 studies. Our methods yield acceptable IW ice volume estimates validating the value of GIS to estimate IW volume on much larger scales. We estimate that IWs are potentially present on 50% of the Fosheim Peninsula (~ 3,000 km^2) where 3.81 % of the top 5.9 m of permafrost could be IW ice.

1 Introduction

Arctic temperatures have increased twice as fast as the rest of the world over the past 50 years; a pattern that is expected to

20 continue for the next century (IPCC, 2013; AMAP, 2017). Permafrost is perennially cryotic ground that is estimated to underlie up to 24 % of the Earth's land surface (French, 2018) including vast areas in the Arctic that are threatened by climate change. Potential feedbacks of thawing permafrost include widespread landscape instability, accelerated coastal erosion and a massive release of carbon into the atmosphere, thus adding to the forcing on Earth's climate through the greenhouse gases effect (Schuur et al., 2015). The Canadian High Arctic permafrost is vulnerable to even a slight temperature increase because it lacks

25 insulation from vegetation. Subsequent melting of ground-ice reinforces the disturbance on permafrost's thermal equilibrium. These effects are already seen in the form of increased subsidence and rapid melting events (Pollard et al., 2015). Ice wedges (IWs), wedge shaped bodies of nearly pure ice, are a ground-ice type ubiquitous in the High Arctic and in areas of continuous permafrost in general. Investigating the response of IWs to climate change is a necessity to understand future permafrost degradation.

1.1 Ice Wedges and Thermokarst

The main factors controlling permafrost occurrence and depth of the active layer are: air temperature, vegetation cover, soil type, snow cover and topography (French, 2007). Thermokarst refers to all the processes related to permafrost degradation involving subsidence, erosion, collapse and instability resulting from thawing of ice-rich permafrost or the melting of massive ice (van Everdingen, 1998). Ice-rich permafrost typically contains ice contents well in excess of the saturated moisture content of the sediments under natural unfrozen conditions (van Everdingen, 1998); the volume of ice in excess of saturation is called excess ice. Thermokarst is initiated when the thermal equilibrium of permafrost is disrupted as a result of increasing ground surface temperature which causes warming the upper part of the permafrost and increasing the depth of the active layer. Thermokarst alters surface hydrology favouring pond formation and gully formation, further causing permafrost erosion and thaw (Godin and Fortier, 2012). The magnitude of thermokarst driven geomorphic change is highly dependent on ground-ice content (Couture and Pollard, 2007; Kokelj and Jorgenson, 2013; Pollard et al., 2015). Thermokarst features can be geomorphologically significant in landscapes containing massive ground-ice and IW ice. These permafrost features have the highest excess ice contents since they are usually composed of almost pure ice (Couture and Pollard, 1998) (Fig. 1).

Rapid cooling of soil can lead to thermal contraction and result in crack formation. At the beginning of the thaw season, contraction cracks are filled with melt water that freezes to form a vertical vein of ice. Over hundreds of years, re-forming cracks create polygonal patterns and form large IWs that are widespread in the Arctic and for this reason has been the subject of abundant research (e.g. Leffingwell 1915; Lachenbruch, 1962; Black, 1976; Mackay, 1990).

Three types of IWs are identified based on their growth direction relative to the ground surface: epigenetic, syngenetic and anti-syngenetic wedges (Mackay, 1990). Epigenetic IWs typically grow on stable surfaces in pre-existing permafrost (Fig. 2). Their V-shape denote their tapered growth as cracks tend to form in the middle of the wedge. Syngenetic IWs grow upward as a response to surface aggradation of sediments. They are typically located in floodplains, where fluvial sedimentation occurs, in areas of eolian sedimentation, and on slopes from the result of mass wasting. They are often nested in a chevron pattern. Anti-syngenetic IWs are characterized by a gradual downward growth pattern because of an incremental removal of surface material, for example on a slope affected by slow mass wasting. They penetrate deeper each year if thermal contraction cracking keeps pace with ice vein formation and their tops are truncated by thaw (Mackay, 1990). In the Canadian High Arctic polar desert, epigenetic IWs are most typical and reflect a dynamic balance between climate and geomorphology whereas the other types are less common and occur in areas of geomorphic change (e.g. deposition and erosion). The distinct polygonal patterns produced by networks of IWs reflect the complex interaction between climate, materials and topography. In general, two polygonal morphotypes are recognized; namely high and low centred polygons depending on the microtopographic relationship between polygon edges and polygon centres (Mackay, 2000). In this study, our analysis is concerned with epigenetic IWs, most commonly expressed as high-centered polygons in polar desert environment.

As IWs grow, a shallow trough often develops over the ice body reflecting the quasi-stable relationship between the active layer and the IW top. In some cases, ridges parallel to the IW trough develop, creating low-centred polygons with raised rims often higher than 50 cm (French, 2007). Preferential thaw of IW happens when snowmelt and runoff collect and flow in IW troughs creating a thermal perturbation. Changes in microtopography related to the evolution of high and low centred IW polygons play an important role in surface process by influencing drainage, snow distribution and vegetation. These changes generate feedbacks that accentuate polygon morphology and eventually their vulnerability to thawing (Liljedahl et al. 2016).

1.2 High Arctic Climate Change

Climate change in the Arctic will impact the three most important environmental factors dictating permafrost and ground-ice state, namely: air temperature, vegetation characteristics and snow cover. Regional interaction between these biological and physical dimensions make it difficult to generalize permafrost response to increased temperatures at the local scale. Decreasing albedo due to diminishing snow cover, glacier ice and sea ice extent affects atmospheric and oceanic circulation amplifying the increase in temperatures in the northern polar region (IPCC, 2013). In the Canadian High Arctic, increase in air temperature has largely resulted in winter and autumn warming, and sites with little snow cover exposed to winds are therefore more responsive to changes in air temperatures (Smith et al., 2012). An increase in annual snow accumulation is also projected for high latitudes due to warmer temperatures (AMAP, 2017). Since the 1980s, permafrost temperatures have risen in most regions, but this increase is particularly strong (0.4 °C to 1 °C per decade) in continuous cold permafrost regions such as the High Arctic (AMAP, 2017). This rise in ground temperature is disturbing the thermal equilibrium of permafrost and result in changes in the active layer thickness and surface conditions. Increased thermokarst processes will enhance the permafrost carbon feedback through the release of greenhouse gases from a previously frozen organic pool (IPCC, 2013). The release of these large carbon and methane reserves will have an important effect on global temperatures on a millennial timescale (IPCC, 2013, Schuur et al., 2015). It is currently estimated that permafrost regions contain twice as much carbon that there is in the atmosphere (Schuur et al., 2015). However, the Canadian High Arctic permafrost is underrepresented in terms of datasets for carbon stocks (Brummell et al., 2014; Schuur et al., 2015). This region is dominated by a polar desert landscape (Walker et al., 2002) where the cold dry soils contains a smaller carbon pool than tundra and it is uncertain if it will stay as a carbon sink (Brummell et al., 2014; Schuur et al., 2015). No clear trend in increase in thermokarst activity linked to climate change in the Arctic has been observed in the past decade (AMAP, 2017). However, widespread IW degradation has been observed in the Canadian Arctic Archipelago, Alaska and Siberia in recent decades and linked to climate change (Liljedahl et al., 2016). As climate change projections specific for the High Arctic polar deserts are poorly constrained due to a lack of data (Pollard et al., 2015), many uncertainties remain about their response to increase in temperature and permafrost stability.

1.3. Ground-ice Volume Estimation

Analysis of permafrost and modelled disturbance due to an increase in ground temperature shows that the "degree of response", specifically the magnitude of ground subsidence, is a direct function of the volume of excess ice (Couture and Pollard, 2007). Ground-ice content is a key property to define permafrost terrain (Gogineni et al., 2014) and its estimation is necessary to predict the sensitivity of a particular area to disturbance (Gilbert et al., 2016), which is important for engineering and environmental evaluations. It is also crucial for quantifying carbon pools and potential fluxes into the atmosphere (Kuhry et al., 2013; Strauss et al., 2013; Ulrich et al., 2014). Understanding the cryostratigraphy and estimating ground-ice type proportions also helps to reconstruct geomorphic history (Couture and Pollard, 2007; Gilbert et al., 2016). One of the first regional ground-ice approximation study was performed by Pollard and French (1980) for Richards Island in the Mackenzie Delta, N.W.T. Estimation of ground-ice in the upper 10 m of permafrost was completed using drill log data, aerial photographs and topographic maps. Field intensive studies to characterize IW terrain and estimate ground-ice content have recently been carried out in the Mackenzie Delta by Morse and Burn (2013) and on the Beaufort Sea coast in Alaska by Kanesvskiy et al. (2013). The lack of detailed field data for large and basically unstudied areas in the Arctic explains why ground-ice distribution is often estimated at small regional scales.

Pore ice and segregated ice volumes can be determined from permafrost sample analysis, but not large ice bodies like wedges and massive ice. To specifically conduct IW volume estimations, knowledge of IW morphology as well as IW polygons geometry are required. Point measurement data from exposed IWs, excavation and/or boreholes helps to constrain IW type, shape and mean IW width and depth for a specific site (e.g. Pollard and French, 1980; Morse and Burn, 2013; Jorgenson et al., 2015). Geophysical techniques such as ground penetrating radar (GPR) and electrical resistivity tomography (ERT) have also been used to investigate IW morphology (e.g. Munroe et al., 2007; Bode et al., 2008; De Pascale et al., 2008; Léger et al., 2017). IW are often approximated to be an inverted isosceles triangle and mean cross-sectional area of IWs is estimated with the use of width to depth ratios based on field observations. This works well for epigenetic and anti-syngenetic IWs but would underestimate syngenetic ice volume due to their chevron pattern (Morse and Burn, 2013). Many other assumptions are often made which lead to over/under-estimation of wedge ice. For example, Kanevskiy et al. (2013) assumed that IW polygons were square and did not take into account the active layer thickness. Pollard and French (1980) adapted their IW volume estimation for areas with less developed polygons to come with an overall volume for Richard Island, N.W.T. Bearing in mind the assumptions made possibility yield large errors, such studies give some crucial information on relative proportion of IW volume as a first approximation.

IW polygon geometry, mainly perimeter and total length of troughs for a defined surface area, can be manually calculated on a small scale from air photos (e.g. Pollard and French, 1980; Couture and Pollard, 1998). Improvements in remote sensing capabilities to do such task is needed to characterize various permafrost regions (Jorgenson and Grosse, 2016). In the review

of recent advances in the study of ground-ice by Gilbert et al. (2016), the use of satellite imagery has been recognized as the main contemporary method to determine IW polygon geometry on larger scales. Access to remotely sensed high-resolution imagery encouraged the development of techniques to measure polygon geometries using Geographic Information Systems (GIS). Ulrich et al. (2014) proposed a method to estimate IW volume from high resolution satellite images and limited ground

5   data using three-dimensional GIS tools. Polygon networks are delineated from satellite imagery and converted into a Triangular Irregular Network (TIN). Average IW width and depth from previous field surveys serve as inputs to a 3D subsurface model of polygons enabling wedge ice volume calculation. Their method was used in Yedoma deposits (Pleistocene-age ice-rich permafrost) and Holocene thermokarst basins in Siberia and Alaska. Two procedures were used to digitize the troughs centrelines in their study: manual delineation and Thiessen polygons delineation. Compared to previous estimation methods,

10   the volume accuracy is increased as the actual polygon dimensions are used. The study by Ulrich et al. (2014) establishes that GIS is an appropriate tool to conduct estimates of geometrically irregular features on a large scale but recognizes that precise field data are necessary.

IWs and in some cases pingos are the only massive ground-ice types that can be mapped using high resolution satellite imagery.

15   Previous studies have shown that IWs occur literally everywhere in unconsolidated sediments in the continuous permafrost zone and that their subsurface geometry is relatively consistent and closely related to terrain conditions and surficial geology (Couture and Pollard, 2007). Given the predicted changes in Arctic climate and our current understanding about nature and distribution of IWs, it is safe to assume that IW melt will contribute greatly to High Arctic geomorphic change with feedbacks that will reinforce permafrost instability. Semi-automated techniques to delineate IW polygons on satellite images would

20   greatly improve time efficiency and coverage area of wedge ice volume estimates compared to manual delineation. In this study, we estimate the volume of ice associated with IWs using a novel GIS approach in a specific region of the Canadian High Arctic, the Fosheim Peninsula. The goals of this study are twofold: (1) build upon the methodology introduced by Ulrich et al. (2014) by testing semi-automated methods to delineate IW troughs and, (2) perform a rough estimation of IW ice volume of the Fosheim Peninsula.

25   **2 Study Area: Fosheim Peninsula**

The Fosheim Peninsula lies within the Eureka Sound Lowlands (ESL), which include the central part of Ellesmere and Axel Heiberg Islands in the northernmost part of the Canadian Arctic Archipelago. Our study focusses on the Fosheim Peninsula on Ellesmere Island (Fig. 3) which lies within the ESL region. Environment Canada weather station located at Eureka (80°00′ N, 85°55′ W) is in the centre of the ESL on the Fosheim Peninsula. The area is flat to gently rolling, at elevations <200 m a.s.l.

30   and the surface is comprised of mostly ice-rich silty-clay marine sediments underlain by continuous permafrost ~500 m deep. This area is characterized as a polar desert and is one of the driest regions in Canada, with a mean annual precipitation of 68 mm recorded at Eureka for the period 1980-2015. The mean annual air temperature is -18.8 °C with the coldest mean monthly

temperature in February of -37.4 °C and warmest in July of 6.2 °C for the same period. The thaw season varies between 3 and 6 weeks in length (Pollard et al., 2015). The mountains surrounding the ESL limit cold air masses from the ocean and create relatively warm July temperatures for this latitude and a general warming trend has been noted for this month since 1980 (Pollard et al., 2015). The mean active layer thickness is 60 cm, and ranges between 30–100 cm. IW polygons are nearly

5   continuous in unconsolidated sediments across the ESL and exposures of thick tabular massive ice bodies are numerous (Pollard et al., 2015). It was estimated that in this region wedge ice accounted for 1.8–3.5 % in volume of the upper 5.9 m of permafrost and that all types of ground ice combined accounted for 30.8 % (Couture and Pollard, 1998). Average IW width is 1.46 m and depth 3.23 m from a survey of 150 exposed IWs by Couture and Pollard (1998). Extreme polar latitudes often lack thermokarst features, but with ice content often exceeding 60–70 % in the fine marine sediments, the ESL is an exception

10   (French, 2007; Pollard et al., 2015). The location is IW very close to the surface makes them vulnerable to an increase in temperature which results in an increase in the active layer thickness. The response of High Arctic polar desert to projected climate change was modelled by Couture and Pollard (2007) with the climatic and geologic conditions of the ESL. They outlined two scenarios of +4.9 °C and +6.6 °C mean annual air temperature increase in the 2040-2060 period compared to mean annual air temperature from the 1948-1997 period. These led to a lengthening of the thaw season by 26 days and increased

15   thaw depths of 17–20 cm. Comparison with modeled and past disturbance values reveal that ground subsidence is on the order of 1 m in the vicinity of IWs and greater than 1 m for massive ground-ice bodies.

3 Methodology

3.1 Data Sources and Sample Areas

To assess the best techniques for IW trough delineation, we first identified a series of suitable sample areas from a detailed

20   analysis of four high resolution (0.5 m pixels) WorldView 2 and 3 satellite images. Like Ulrich et al. (2014) we defined the sample areas as squares of 250x250 m. Four sample areas, three on Ellesmere Island (EL1, 2 and 3) and one on Axel Heiberg Island (AH1) with different polygon size, morphology, density and width of troughs were selected (Table 1 and Fig. 8). All sample areas are characterized by random orthogonal polygons formed by epigenetic IWs on relatively flat surfaces (Fig. 4). The high-centred polygons on the Ellesmere Island sample areas have well-developed troughs (approximately 2–6 m wide).

25   Wedge hierarchy reflected by variability in trough width is most visible in sample area EL1. EL2 was chosen due to its dominance of rectilinear polygons, while EL3 was chosen for the high number of polygons with small areas and their proximity to polygons with much larger areas. In contrast, AH1 was chosen because of polygons with large areas and narrow troughs where cracking is assumed to be less frequent. AH1 is the only sample area where IW cracks not forming closed polygons are visible.

3.2 Delineation of Polygons

At each sample area, the following three delineating methods were performed once using built in tools in ArcGIS (ESRI, Version 10.3.1): (1) Manual delineation, (2) Thiessen polygons and (3) Watershed Segmentation. In our method, we use and refer to specific ArcGIS tools but most GIS packages contain similar tools and functions that could be used to replicate our

5   analysis.

3.2.1 Manual Delineation

Following the Ulrich et al. (2014) methodology, we manually digitized polygons at each sample area by creating a line dataset of the troughs centrelines. Only lines enclosing complete polygons falling within the sample area were kept and visible IW cracks not enclosing any polygons were also mapped.

10   #### 3.2.2 Thiessen Polygons

The second method involved the semi-automated delineation of polygons based on the creation of Thiessen (or Voronoi) polygons. This approach was used in Ulrich et al. (2014) to estimate volume of a relict IW network in baydzherakhs landforms, where IWs had melted and only raised polygon centres remained, and at other sites to compare with manual delineation. Thiessen polygons are defined mathematically as the perpendicular bisectors of the lines between all input points. Then, the

15   area inside one Thiessen polygon is closer to its associated input point than any other input point (Aurenhammer, 1991). The tool "Create Thiessen Polygon" was used to create Thiessen polygons from manually chosen centre points of IW polygons, hereafter called the "approximated" centre points. Following this creation, polygons near the outer boundaries of the sample squares were necessarily defined by having these boundaries as vertices. To avoid those edge effects, we created approximated centre points for polygons up to 30 m away from the sample areas before the creation of the Thiessen polygons. All resulting

20   polygons that were not completely inside the sample areas were then deleted, and the remaining polygons were converted to a line dataset. Approximated centre points were created without the manual delineation lines visible to test the ability of the analyst to identify IW polygon centres.

3.2.3 Watershed Segmentation

Delineating IW polygons has many similarities with detecting grain boundaries in thin sections for petrographic analysis

25   because both involve detecting edges. In a study by Barraud (2006) grain boundaries are detected using a "Watershed Segmentation" algorithm in image segmentation software. The basic principles of this segmentation process were reproduced in this study with the Spatial Analyst Hydrology toolbox of ArcGIS.

This third delineation method is based on the interpretation of the value of each pixel as a height function, i.e. as if it was a

30   Digital Elevation Model (DEM). If the IW troughs have higher pixel values (brighter) than the polygon centres they will act

as "mountains" and polygon centres as "valleys". If this topography was to be flooded, the water would accumulate in each polygon centre "valley" delineated by the trough boundary "mountains". In the WorldView images, the polygon centres have higher value pixels and the troughs lower value, therefore we inverted the pixel values before using the hydrology tools.

5 Watersheds were first obtained using the "Flow Direction" tool to calculate the flow direction of each pixel in the image, and then the "Basin" tool was used to delineate the smallest possible watersheds where water could accumulate. We converted the multiple steps of this method into a semi-automated process by implementing them in ArcGIS Model Builder (Fig. 5), which increased time-efficiency and required few interventions from the analyst. Filtering and smoothing of the image is required before the "Flow Direction" and "Basin tool" outputs can provide watershed outlines that are representative of the IW polygons
10 (Fig. 5a). To enhance troughs pattern, we used the "Focal Statistic Maximum" tool followed by the "Focal Statistic Mean" tool to reduce noise in the polygon centres. The later had to be performed multiple times to generate watersheds that were not over segmented, i.e. too many watersheds representing one actual IW polygon. Watersheds were created after each focal mean iteration and evaluated against the manually digitized polygons lines. The iterations were stopped when some watersheds started to merge and to include two or more manually digitized polygons. At this point, approximately one to eight watersheds
15 represented each actual IW polygon.

The hydrology tools were used on all of the available bands in WorldView imagery at each sample areas (Table 1) before being combined into a single line dataset per sample area. The same number of focal mean iterations were performed on all the bands and they were then combined to create the final IW polygon delineation lines. For each band, watershed outlines
20 were extracted as lines and were converted into a raster format (Fig. 5b). The three raster datasets of each band were summed, and pixels which were classified as boundaries (IW troughs) in two or more of the bands were kept (Fig. 5c). For these steps, the pixel size was increased from 0.5 to 1 m to get better chances of the watershed outlines overlapping. To convert the boundary pixel raster into a clean line dataset, the output raster was thinned, watershed boundary pixels converted to polylines, and the "Extend Line" tool used with a maximum extension distance of 5 m (10 original pixels) to obtain a maximum number
25 of closed polygons.

The clean trough centrelines datasets representing IW polygon outlines were visually assessed and edited to improve their accuracy. With the initial WorldView image visible, lines over-segmenting the IW polygons were deleted and lines were added where polygons when some boundaries were not closed. All lines outside the sample areas were also deleted. Manually
30 delineated polygons were included in these edited datasets to be consistent with the initial choice of the analyst. The remaining dangling lines were erased using the "Trim Line" tool. Finally, the "Simplify Line" tool with the point remove option and a tolerance of 1.5 m (3 pixels) was used to smooth any lines which had sharp edges due to the contouring of pixels form the conversion of raster to polyline format.

3.3 Three-dimension Subsurface Model for Ice Wedge and Sediment Volume Calculation

Similar to Ulrich et al. (2014) field data of mean IW depth and width were used to estimate IW volume, here from Couture and Pollard (1998). A buffer was created around the delineated lines of half the mean width of an IW (0.73 m) and then the buffer extent was cut out of the polygons with the "Erase" tool. The resulting polygons therefore did not include the IW troughs. All polygons, even the edge ones, are then considered to be surrounded by half an IW.

Volume calculations were performed in a 3D subsurface model by creating a Triangulated Irregular Network (TIN) dataset, which is a network of mass points representing a surface terrain. Assuming that the IWs are inverted isosceles triangles, the elevation of -3.23 (mean IW depth) was assigned to the trough centrelines and an elevation of 0 was assigned to the polygons corresponding to the base of the active lapyer (see legend for elevation in Fig. 6). An elevation of -3.23 was also assigned to a dissolved polygon extent. The TIN was created from those three datasets with the Delaunay triangulation constrained for each segment (lines and polygon vertices) to be added as an edge in the TIN.

The IW volume and sediment volume were calculated using the "Surface Volume" tool. The IW volume was calculated from a plane above the TIN at 0 m. In order to compare the results of this study with the values found in Couture and Pollard (1998), the thickness of frozen soil considered in their study (5.9 m) was used to calculate sediment volume. It was calculated from a plane at this depth below the TIN (-5.9 m). The percent volume of IWs at each sample area was calculated by dividing the IW volume by the total frozen material (sediment and IWs) volume.

3.4 Fosheim Peninsula Ice Wedge Volume Estimation

We estimated the cumulative coverage area of IW polygons for the Fosheim Peninsula based on the surficial geology map from Bell (1992). The map was digitized with reference to the shoreline and contour datasets of CanVec series dataset from Natural Resource Canada (2016). As it is rare for IW polygons to occur in bedrock (French, 2007), it was assumed that they can be located only in unconsolidated surficial sediments (marine, fluvial, glacial sediments). The potential area occupied by IWs was determined by subtracting the area of the large lakes and intact bedrock areas. The 150 m CanVec contour was isolated as this provides a proxy for the Holocene marine limit on the Fosheim Peninsula because IWs are ubiquitous below this elevation (Bell, 1996; Couture and Pollard, 1998). We assumed that the mean of the IW percent volume of our sample areas was representative of the geomorphological settings on Fosheim Peninsula and used it to calculate the equivalent IW ice volume over the entire peninsula.

4 Results

4.1 Delineation of Polygons

To compare the accuracy of the two semi-automated delineation methods against the manual method, the mean perimeter and area of polygons (Fig. 7a) as well as the total length of delineated troughs (Table 2) were calculated. It is expected that a more

5 efficient method would have a mean perimeter and mean centre point distance close to the manual delineation method values.

All the delineation methods provided polygon outlines for the four sample areas, although the accuracy of the outlines is variable. We assume that the manual method provides the best outlines because troughs can be detected by the analyst regardless of their width and intersection with other troughs. Manually delineating the troughs was most difficult at EL3 where

10 polygons were small and contrast was very low especially on the left side of the sample area (Fig. 4). Presence of IW troughs that do not form closed polygons in AH1 were also difficult to detect as the troughs themselves were thin. When compared with the manual trough centrelines, the Thiessen polygons do not agree very well as they simplify the actual polygon shapes. Some edge effects remain on the Thiessen polygon boundaries, mostly caused by the proximity of polygons with large area difference (Fig. 4). The number of polygons were slightly increased at EL2 (+3.57%) and EL3 (+0.04%) and equal at EL1 and

15 AH1 for the Thiessen polygons method (Table 2). The edited trough centrelines from the Watershed Segmentation method are generally in good agreement with the manually digitized trough centrelines (Fig. 4). The Watershed Segmentation technique overestimates the number of polygons, by as much as 5 times in the case of AH1 but around two times for the three Ellesmere Island sample areas (Table 2). This result is anticipated as watershed over segmentation is preferred to under segmentation before editing, because outlines of smaller polygons would disappear when watersheds would start to merge.

The mean distance between the centre points of the polygons for the different methods was calculated as an indicator of the similarity between the delineated polygons, particularly for the Thiessen approximated centre points versus the manual centre points (Fig. 7b). At all sample areas, this mean distance is <4 m, equivalent to <8 pixels. The maximum distance encountered was 9.5 m for a polygon on the edge of EL2 for the Thiessen polygons method. Two patterns in the mean distance between

25 centre points seem to emerge: (1) the grouping of Manual/Thiessen Approximated with Manual/Watershed Segmentation and of Thiessen/Thiessen Approximated with Manual/Thiessen due to their value closeness, and (2) the fact that the last group has higher values. The only exception to this observation is the Manual/Watershed Segmentation mean distance being the highest value for EL3.

30 The mean perimeter and polygon areas of the Thiessen and Watershed Segmentation methods have in majority a difference of <5 % with the manual method at a given sample area (Fig. 7a). Exceptions occur at larger polygon sample areas with the Thiessen polygons method, where polygon area is overestimated by 11.6 % and 15.5 % for EL2 and AH1, respectively (Fig. 6a). Another exception occurs for mean perimeter of polygons at AH1, where it is underestimated by >10 % for each method

(Fig. 7a). The Thiessen method overestimates the mean polygon area at each sample area, with proportionally greater overestimations for sample areas with larger polygons. The Watershed Segmentation area estimation is more precise, being <1 % different than the mean area for the manually delineated polygons at all sample areas.

4.2 Ice Wedge Volume

An example of the TIN output for the IW volume calculation can be found in Fig. 6. The percent volume of IWs in the top 5.9 m of frozen material ranges from 1.41 %, for the lowest polygon density AH1, to 5.88 % for the highest polygon density sample area EL3, all delineation methods included (Table 2). IW volumes for the Watershed Segmentation and Thiessen methods are slightly lower or equal to the manual method estimate. The largest difference occurs at AH1 where there is a difference of -0.31 in the percent IW volume, which is equivalent at this sample area to 7.23 m^3 of IW ice. At each sample area, the IW volume estimate from the Thiessen polygons method is the lowest except in the case of EL1 where it is equal with the Watershed Segmentation method, but still lower than the manual method estimates (Table 2).

Based on digitization of the Bell (1992) map, approximately half of the Fosheim Peninsula surface area contains IWs, corresponding to an area of ~3,000 km^2 (Fig. 8). Considering only the top 5.9 m of permafrost, this is equivalent to a volume of frozen material of 17.7 km^3. The total IW ice volume is $6.7x10^8$ m^3, when assuming an IW volume of 3.81 % by averaging the results from the manual delineation at the four sample areas in Table 2.

5 Discussion

5.1 Semi-automated Delineation Methods

The use of the Thiessen method on four sample areas with various polygon morphologies reveals its strength for volume estimation but not for trough identification. Indeed, the main problem with this method is that curved troughs could not be delineated properly because the "Create Thiessen Polygon" tool can only output straight lines. This is reflected by the overestimation of polygon area (Fig. 7a). It is anticipated that better results would be obtained for hexagonal or rectangular polygonal patterns, rather than the orthogonal polygons tested in this study. This method is the least time consuming, but overall it underestimates IW volume by differing between 0.1-0.3 % from the percent IW volumes from manual delineation (Table 2). The Thiessen method was judged by Ulrich et al. (2014) to be "visually similar" to manual digitization. However, their study areas had a majority of rectilinear polygons, for which the approximation of centre point is easier than for more complex shapes found in the sample areas used for this study.

The Watershed Segmentation method developed for this study with ArcGIS Hydrology tools was the most accurate in terms of locating trough centrelines and IW volume for every sample area. The poor agreement along the margins of sample area EL3 can be attributed to the lack of contrast in this part of the image (Fig. 4), and explains why the mean distance between the

automatically vs. manually derived centre points is the highest at this sample area (Fig. 7a). With minimal editing, the IW volume calculations using the Watershed Segmentation results were equal to the manual method values for two sample areas. The method accuracy can be improved by editing the sharp angles at boundaries that are not completely smoothed with the "Simplify Line" tool. These are most prevalent at sample area AH1 where the XY tolerance to simplify the lines (1.5 m) was the smallest compared to the polygon vertices length. The accuracy of the trough centreline positions was reduced when increasing the pixel resolution to 1 m in the "Polyline to Raster" conversion but does not make a large difference in IW volume as the troughs are overwhelmingly larger than 1 m (2 pixels) at every sample area.

The effect of larger polygon size is visible in the results of sample area AH1 with the greatest differences in mean perimeter and area of polygons compared to manual delineation, and this independently of the method used. This can also be attributed to the thin troughs at this sample area and to the difficulty of differentiating what seems like dry runoff channels from IW troughs (Fig. 4).

This study focussed on the development of two methodologies to delineate IW polygons based on only four sample areas. However, we are confident that both methods are applicable to delineating polygons for much larger areas. Thiessen polygons can readily be generated for larger areas and manually edited along the boundaries to reduce edge effects. The Watershed Segmentation method can also be used for larger areas by choosing a number of focal mean iterations that will preserve the boundary details of the smallest polygons present. Even if over-segmented, this method preserves the largest polygon outlines corresponding to the darker zones of the images, interpreted as higher elevation when creating watersheds. However, the applicability of this methodology on terrain with complex contrast patterns in satellite imagery has not been tested. We suspect that presence of water bodies in IW polygons or troughs or of prominent vegetation at lower Arctic latitudes would impact the proper detection of IW troughs. Hence, we suggest that it could be applied on high resolution DEMs (>0.5 m horizontal and vertical accuracy) instead of high resolution satellite images. Then, the Watershed Segmentation method would be applicable with more confidence on a wider range of Arctic terrain. The need of higher resolution DEMs has been identified for the study of permafrost degradation in general, to monitor surface subsidence and thermokarst processes (Jorgenson and Grosse, 2016). Promising remote sensing methods to detect topographic and subsurface change and to map ground-ice distribution include: airborne light detection and ranging (LiDAR), interferometric Radar (InSAR), airborne ground penetrating radar and structure-from-motion technology (Gogineni et al., 2014; Jorgenson and Grosse, 2016). High resolution terrain models can be derived from these methods that are needed to monitor surface subsidence at a smaller scale and to estimate ground-ice distribution over large areas (Gogineni et al., 2014). These data could be acquired from unmanned aerial vehicles (UAVs) or other airborne platforms and would require fieldwork. This highlights the strength of our relatively simple methodology that can be applied on remote locations without the need of extensive fieldwork.

There are other semi-automated delineation methods that could be used to improve the delineation process of IW polygons on satellite images. One potential technique is the method described by Li et al. (2008), which was used to delineate grain boundaries in rock thin sections. In this method, edge detection is based on the abrupt change in pixel values, representing brightness, at the boundary between two grains. However, this method was deemed unsuitable for delineation of IW polygons since it requires considerable manual editing, and image classification algorithms could also not be applied due to the lack of contrast in some of our satellite images. Another approach would be to build on the methodology of Skurikhin et al. (2013) who classified Arctic tundra drainage network components including IW troughs with image segmentation and shape-based classification.

5.2 Ice Wedge Volume Calculations

IW volume derived from manual delineation at the four sample areas of this study are similar to the results of Couture and Pollard (1998) on the Fosheim Peninsula. Their study concluded that for "low density" polygonal terrain IW ice comprised 1.8 % of the top 5.9 m of permafrost and "high density" polygonal terrain 3.5 %. Their low density sample is very close to sample area AH1 (1.73 %), which confirms that the sample area on Axel Heiberg Island is representative of parts of the Fosheim Peninsula. Even if our values from EL2 are very similar to the "high density" values in their study, EL1 and EL3 have a much higher IW ice volume percentage, redefining "high density" polygonal terrain on the Fosheim Peninsula. This may be due to the choice of sample areas of 250x250 m for estimating IW volume. This surface area was found by Ulrich et al. (2014) to provide a representative scale where polygon diameter showed only small variations. Although, the polygon density and shapes of sites in Siberia used by Ulrich et al. (2014) may not be comparable to the sites tested here this size was chosen in our study as a manageable area for manual delineation and development of methodologies to delineate polygons. In future studies, the effect of scale of the extent considered on the IW perimeter, area and IW volume should be assessed to refine the IW volume estimation.

Multiple necessary assumptions are made when calculating IW volume with TINs and here we consider their potential effect in estimating IW volume at large scales. It was assumed that IW width and depth does not vary significantly between polygonal terrains, and lack of subsurface data means that using mean IW width and depth is the best approximation we can use for our calculations. However, one example where this assumption is not valid on the Fosheim Peninsula is in the surficial geology unit of thin veneer of glacial sediments identified by Bell (1992). The thickness of this geological unit over bedrock is defined as 2 m, which is less than the 3.23 m mean IW depth used here. This mean IW depth is a minimal estimate because only exposed IWs were measured by Couture and Pollard (1998). Like was done in their study, we used the depth of 5.9 m below the active layer to calculate the IW volume because no IWs were observed below this depth. The assumed fixed geometry of IWs as being isosceles triangles also impacts our IW volume calculation. It is the general shape of epigenetic IWs recognized by Mackay (1990) and the shape used in previous IW volume estimates (e.g. Pollard and French, 1980; Couture and Pollard,

1998; Bode et al., 2008; Ulrich et al., 2014). Even though IWs can be irregularly shaped in cross-section, an inverted isosceles triangle with its base corresponding to the IW width is the best approximation for shape for a calculation of this nature. Based on nearly 20 years of fieldwork on the Fosheim Peninsula, we have found syngenetic IWs relatively uncommon, and limited to areas of active sedimentation like glacial forelands (floodplains), alluvial fans and deltas. Assuming that all IWs in the
5 Fosheim Peninsula were epigenetic should therefore not affect largely our IW volume calculation.

IWs may contain gas inclusions, small amounts of sediment as disseminated grains and discontinuous veins of silt and fine sand (French, 2007). Inclusion of this factor in our volume calculation is not realistic for this first approximation study so it was assumed that IW were all composed of pure ice. This has also been assumed by Ulrich et al. (2014) and most previous
10 studies (e.g. Pollard and French, 1980; Couture and Pollard, 1998; Bode et al., 2008). Delineating IW polygons on satellite images implicitly assumes that all IWs have a visible surface expression (i.e. a trough structure). Field observations in the ESL show that this is not always the case (Pollard et al., 2015) (Fig. 1a) and would lead to an underestimation of IW volumes. The opposite is also true as there might not be an IW below every crack and trough, but our estimates can only be based on what is visible in the satellite imagery.

15 **5.3 Impacts of Melting Ice Wedges**

IWs are the most widespread ground-ice phenomenon in areas of continuous permafrost. By virtue of their formative processes, the top of the active IW in many cases corresponds with the base of the active layer. Since they are in a quasi-stable relationship with maximum seasonal thaw depth, then any increase in the active layer depth will result in a subsidence of the ground surface over the top of the IW. Over time, warmer summers produce small amounts of thaw at the top of the wedge leading to the
20 formation of a shallow trough that marks the long axis of the wedge and emphasizes their polygon geometry. Under stable permafrost conditions, networks of shallow IW troughs will interact with snow distribution, surface vegetation and surface hydrology; in some cases, contributing locally to additional deepening and surface ponding (Jorgenson et al., 2006, 2015). Hence, the localized degradation of IWs may be part of the normal evolution of permafrost landscapes. However, the widespread deepening of the active layer expected under projected Arctic climate change scenarios will lead to dramatic
25 regional changes in landscapes marked by increased local topography and changes in surface hydrology (Liljedahl et al., 2016). As IWs melt out, the sides of the wedge will collapse into the open trough producing a highly dissected landscape characterized by mounds at the former polygon centres and networks of deep channels and shallow ponds along the former IW troughs (Couture and Pollard, 2007).

30 There is evidence that this is already beginning to occur on the Fosheim Peninsula (Fig. 1). An increase in thermokarst processes and retrogressive thaw slump retreat in the ESL over the past 25 years has been documented by Pollard et al. (2015). Unlike IW degradation triggered by associated mainly with thermal erosion by running water (e.g. Fortier et al., 2007), the instability of IWs in this region is related initially to thaw-induced surface collapse, undoubtedly running water will play a role

at some point. The active melt out seen in Fig. 1b gives an indication of how rapid these changes may occur once the system becomes unstable. There is not only subsidence in the IW troughs, but also widespread back wasting of exposed IWs similar to the headwall retreat in a retrogressive thaw slump (Fig. 1a). There is also evidence of shallow active layer detachments along IW troughs in the ESL (Fig. 1b). In some cases, we have observed on the Fosheim Peninsula rapid melt out of IWs
5   contributing to the formation of much larger retrogressive thaw slumps in areas where massive ground-ice is present (Fig. 3a, d). The net result will be a period of landscape instability amplified by feedbacks associated with runoff (surface hydrology), snow accumulation, changing vegetation, thermokarst from massive ground-ice, mass wasting, and microclimate. In principle, the new landscape will develop a deeper active layer consistent with the summer thaw conditions, though it may be long for the new active layer depth to stabilize, prolonging the period of thermokarst activity and subsidence. The new landscape will
10 be quite different and depending on the topographic and geologic setting not unlike a badlands. For other areas, the new landscape will reflect a geomorphic system affected not only by IW degradation but other changes to the permafrost system and surface hydrology.

6 Conclusion

IWs are the most common form of ground-ice in areas underlain by continuous permafrost. The occurrence of IWs increase
15 the biophysical complexity of permafrost landscapes. Their widespread nature will contribute to significant permafrost instability once thermokarsts processes are initiated. IWs exist in a quasi-stable equilibrium with seasonal thaw as defined by the depth of the active layer. Accordingly, a climate change driven increase in active layer depths will likely produce widespread instability of landscapes associated with melting IWs. To better understand the potential impact of widespread destabilization polygonal terrains there is a need to assess the volume and extent of IW ice. In the absence of detailed field
20 observations, the analysis of IW polygons using high resolution satellite imagery and GIS based tools is the most logical solution. Based on our analysis of IW polygons for the Fosheim Peninsula we present three main conclusions. Firstly, with minimal field data two semi-automated methods permit an acceptable approximation of IW volume in remote sample areas of the Arctic. The two GIS-based delineation techniques ─ the Thiessen polygons methodology presented in Ulrich et al. (2014) and the Watershed Segmentation methodology, newly developed in this study ─ yield acceptable IW volume estimates
25 compared to manual delineation. Implementation of these methods in a coded process accelerated the polygon delineation and demonstrates their potential to be applied to much larger areas in an efficient manner. Time constraint and required level of precision in the estimation of IW volume are two criteria to be considered when choosing one of these methods for future application in other sample areas. Secondly, IWs potentially cover an area of ~3,000 km^2 on the Fosheim Peninsula where 3.81% of the upper 5.9 m of permafrost is comprised of IW ice. We limit our calculation to the Fosheim Peninsula to correspond
30 with available information on surficial geology; however we are confident that our results are applicable to the entire ESL. Thirdly, further study in the ESL should focus on estimating IW volume for other sample areas using one of the semi-automated methods to increase the statistical significance of the results. Fieldwork in the ESL region could improve the IW volume

estimates by linking surficial geology and physiographic units with IW characteristics. Associated with estimations of content of other types of ground-ice, carbon content estimation, IW volume estimates will help to assess the vulnerability of High Arctic permafrost to climate change.

Data availability

5   The data used are listed in the references and tables.

Competing interests

The authors declare that they have no conflict of interest.

Acknowledgments

The authors acknowledge the support of ESRI Canada by awarding financial and technical support to C. Bernard-
10   Grand'Maison to complete this project through the McGill University ESRI Canada Award 2016.This research was funded by the Canadian National Science and Engineering Research Council Discovery, Accelerator and Northern Supplement grants awarded to W. Pollard and a Polar Knowledge Canada Northern Scientific Training program grant awarded to C. Bernard-Grand'Maison. The writers would like to acknowledge the logistical support provided by the Polar Continental Shelf Program, Natural Resources Canada. The authors wish to acknowledge discussions with M. Templeton.

15   **References**

AMAP: Snow, Water, Ice and Permafrost in the Arctic (SWIPA) 2017, Arctic Monitoring and Assessment Programme (AMAP), Oslo, Norway. xiv + 269 pp, 2017.

Aurenhammer, F.: Voronoi diagrams — a survey of a fundamental geometric data structure. ACM Computing Surveys
20   (CSUR), 23(3), 345-405. doi:10.1145/116873.116880, 1991

Barraud, J.: The use of watershed segmentation and GIS software for textural analysis of thin sections, J. Volcanol. Geoth. Res., 154(1), 17-33, doi: 10.1016/j.jvolgeores.2005.09.017, 2006.

Bell, T.: Glacial and sea level history of western Fosheim Peninsula, Ellesmere Island, Arctic Canada, Ph.D. thesis, University of Alberta, Edmonton, Alberta, 1992.

25   Bell, T.: The last glaciation and sea level history of Fosheim Peninsula, Ellesmere Island, Canadian High Arctic, Can. J. Earth. Sci., 33(7), 1075-1086, doi: 10.1139/e96-082, 1996.

Black, R. F.: Periglacial features indicative of permafrost: ice and soil wedges, Quaternary Res., 6(1), 3-26, doi: 10.1016/0033-5894(76)90037-5, 1976.

Bode, J. A., Moorman, B. J., Stevens, C. W., and Solomon, S. M.: Estimation of ice wedge volume in the Big Lake area, Mackenzie Delta, NWT, Canada, in: Proceedings of the 9th International Conference on Permafrost, Fairbanks, Alaska, pp. 131-136, 2008.

Brummell, M. E., Farrell, R. E., Hardy, S. P., and Siciliano, S. D.: Greenhouse gas production and consumption in High Arctic deserts. Soil Biol. Biochem., 68, 158-165, doi: 10.1016/j.soilbio.2013.09.034, 2014.

Couture, N. J., and Pollard, W. H.: (1998). An assessment of ground ice volume near Eureka, Northwest Territories. In Proceedings of the 7th International Conference on Permafrost, Yellowknife, N.W.T., pp. 195-200, 1998..

Couture, N. J., and Pollard, W. H.: Modelling geomorphic response to climatic change. Climatic Change, 85(3), 407-431, doi: 10.1007/s10584-007-9309-5, 2007.

De Pascale, G. P., Pollard, W. H., and Williams, K. K.: Geophysical mapping of ground ice using a combination of capacitive coupled resistivity and ground-penetrating radar, Northwest Territories, Canada. J. Geophys. Res. Earth, 113(F2), doi: 10.1029/2006JF000585, 2008.

Fortier, D., Allard, M., and Shur, Y.: Observation of rapid drainage system development by thermal erosion of ice wedges on Bylot Island, Canadian Arctic Archipelago. Permafrost Periglac., 18(3), 229–243. doi:10.1002/ppp.595, 2007.

French, H. M.: The periglacial environment (4th 3rd ed.), John Wiley and Sons, Chichester, England, 201807.

Gilbert, G. L., Kanevskiy, M., and Murton, J. B.: Recent advances (2008–2015) in the study of ground ice and cryostratigraphy, Permafrost Periglac., 27(4), 377-389, doi: 10.1002/ppp.1912, 2016.

Godin, E., and Fortier, D.: Fine scale spatio-temporal monitoring of multiple thermo-erosion gullies development on Bylot Island, Eastern Canadian Archipelago, in: Proceedings of the 10th International Conference on Permafrost, Salekhard, Russia, pp.125-130, 2012.

Gogineni, P., Romanovsky, V.E., Cherry, J., Duguay, C., Goetz, S., Jorgenson M.T., and Moghaddam, M.: Opportunities to use remote sensing in understanding permafrost and related ecological characteristics, in: National Research Council workshop. National Academies Press, 2014.

IPCC: Climate Change 2013: The Physical Science Basis, Contribution of Working Group I to the Fifth Assessment Report of the Intergovernmental Panel on Climate Change, edited by: Stocker, T. F., Qin, D., Plattner, G.-K., Tignor, M., Allen, S. K., Boschung, J., Nauels, A., Xia, Y., Bex, V., and Midgley, P. M., Cambridge University Press, Cambridge, United Kingdom and New York, NY, USA, 1535 pp., 2013.

Jorgenson, M. T., Shur, Y. L., & Pullman, E. R.: Abrupt increase in permafrost degradation in Arctic Alaska. Geophysical Research Letters, 33(2), 2006.

Jorgenson, M., and Grosse, G.: Remote sensing of landscape change in permafrost regions, Permafrost Periglac., 27(4), 324–338, doi:10.1002/ppp.1914, 2016.

Jorgenson, M.T., Kanevskiy, M., Shur, Y., Moskalenko, N., Brown, D.R.N., Wickland, K., Striegl, R. and Koch, J.: Role of ground ice dynamics and ecological feedbacks in recent ice wedge degradation and stabilization, J. Geophys. Res. Earth, 120(11), 2280-2297, doi: 10.1002/2015jf003602, 2015.

Kanevskiy, M., Shur, Y., Jorgenson, M.T., Ping, C.L., Michaelson, G.J., Fortier, D., Stephani, E., Dillon, M. and Tumskoy, V.: Ground ice in the upper permafrost of the Beaufort Sea coast of Alaska, Cold Reg. Sci. Technol., 85, 56-70, doi:10.1016/j.coldregions.2012.08.002, 2013.

Kokelj, S. V., and Jorgenson, M. T.: Advances in thermokarst research, Permafrost Periglac., 24(2), 108–119, doi:10.1002/ppp.1779, 2013.

Kuhry, P., Grosse, G., Harden, J.W., Hugelius, G., Koven, C.D., Ping, C.L., Schirrmeister, L. and Tarnocai, C.: Characterisation of the permafrost carbon pool, Permafrost Periglac., 24(2), 146-155, doi: 10.1002/ppp.1782, 2013.

Lachenbruch, A. H.: Mechanics of thermal contraction cracks and ice-wedge polygons in permafrost, Geol. S. Am. S.,70, 1-66, doi: 10.1130/SPE70-p1, 1962.

Leffingwell, E. de K.: Ground-ice wedges the dominant form of ground-ice on the north coast of Alaska: Jour. Geology, v. 23, no. 7, p. 635-654, 1915.

Léger, E., Dafflon, B., Soom, F., Peterson, J., Ulrich, C., and Hubbard, S.: Quantification of arctic soil and permafrost properties using ground-penetrating radar and electrical resistivity tomography datasets, IEEE J. Sel. Top. Appl., 10(10), 4348-4359, doi: 10.1109/JSTARS.2017.2694447, 2017.

Li, Y., Onasch, C. M., and Guo, Y.: GIS-based detection of grain boundaries, J. Struct. Geol., 30(4), 431-443, doi: 10.1016/j.jsg.2007.12.007, 2008.

Liljedahl, A.K., Boike, J., Daanen, R.P., Fedorov, A.N., Frost, G.V., Grosse, G., Hinzman, L.D., Iijma, Y., Jorgenson, J.C., Matveyeva, N. and Necsoiu, M.: Pan-Arctic ice-wedge degradation in warming permafrost and its influence on tundra hydrology. Nat. Geosci., 9(4), 312-318, doi: 10.1038/ngeo2674, 2016.

Mackay, J. R.: Some observations on the growth and deformation of epigenetic, syngenetic and anti-syngenetic ice wedges, Permafrost Periglac., 1(1), 15-29, doi:10.1002/ppp.3430010104, 1990.

Mackay, J. R.: Thermally induced movements in ice-wedge polygons, western arctic coast: a long-term study, Géogr. Phys. Quatern., 54(1), 41-68, doi:10.7202/004846ar, 2000.

Morse, P. D., and Burn, C. R.: Field observations of syngenetic ice wedge polygons, outer Mackenzie Delta, western Arctic coast, Canada, J. Geophys. Res. Earth., 118(3), 1320-1332, doi: 10.1002/jgrf.20086, 2013.

Munroe, J.S., Doolittle, J.A., Kanevskiy, M.Z., Hinkel, K.M., Nelson, F.E., Jones, B.M., Shur, Y. and Kimble, J.M.: Application of ground-penetrating radar imagery for three-dimensional visualisation of near-surface structures in ice-rich permafrost, Barrow, Alaska, Permafrost Periglac., 18(4), 309-321, doi: 10.1002/ppp.594, 2007.

Natural Resources Canada: CanVec, last access: 2016, available at: http://geogratis.gc.ca/site/eng/download

Pollard, W. H., and French, H. M.: A first approximation of the volume of ground ice, Richards Island, Pleistocene Mackenzie Delta, Northwest Territories, Canada. Can. Geotech. J., 17(4), 509-516, doi: 10.1139/t80-059, 1980.

Pollard, W., Ward, M., and Becker, M.: The Eureka Sound Lowlands: an ice-rich permafrost landscape in transition, in: Proceedings of GeoQuebec 2015, 68th Canadian Geothechnical Conference and 7th Canadian Permafrost Conference, Quebec, QC., 2015.

Schuur, E.A.G., McGuire, A.D., Schädel, C., Grosse, G., Harden, J.W., Hayes, D.J., Hugelius, G., Koven, C.D., Kuhry, P., Lawrence, D.M. and Natali, S.M.: Climate change and the permafrost carbon feedback. Nature, 520(7546), 171-179, doi: 10.1038/nature14338, 2015.

Skurikhin, A. N., Gangodagamage, C., Rowland, J. C., and Wilson, C. J.: Arctic tundra ice-wedge landscape characterization by active contours without edges and structural analysis using high-resolution satellite imagery, Remote Sens. Lett., 4(11), 1077-1086, doi: 10.1080/2150704X.2013.840404, 2013.

Smith, S. L., Throop, J., and Lewkowicz, A. G.: Recent changes in climate and permafrost temperatures at forested and polar desert sites in northern Canada, Can. J. Earth. Sci., 49(8), 914-924, doi: 10.1139/e2012-019, 2012.

Strauss, J., Schirrmeister, L., Grosse, G., Wetterich, S., Ulrich, M., Herzschuh, U., and Hubberten, H. W.: The deep permafrost carbon pool of the Yedoma region in Siberia and Alaska. Geophys. Res. Lett., 40(23), 6165-6170, 2013.

Ulrich, M., Grosse, G., Strauss, J., and Schirrmeister, L.: Quantifying Wedge-Ice Volumes in Yedoma and Thermokarst Basin Deposits. Permafrost Periglac., 25(3), 151-161, doi: 10.1002/ppp.1810, 2014.

Van Everdingen, R. (Eds.): Multi-language glossary of permafrost and related ground-ice terms, National Snow and Ice Data Centre, Boulder, CO, 1998.

Walker, D. A., Gould, W. A., Maier, H. A., and Raynolds, M. K.: The Circumpolar Arctic Vegetation Map: AVHRR-derived base maps, environmental controls, and integrated mapping procedures, Int. J. Remote Sens., 23(21), 4551-4570, doi: 10.1080/01431160110113854, 2002.

Tables

Table 1. Definition of the sample areas and satellite imagery used

Sample area	Image name, Date	Satellite	Sample area extent (top left corner)	No. of bands used (description)
Ellesmere Island 1 (EL1)	Slidre Fjord, 01/07/2012	WorldView 2	80˚00'28.7892'' N 85˚50'28.5809'' W	1 (Panchromatic Band)
Ellesmere Island 2 (EL2)	Slidre Fjord South 15, 08/09/2015	WorldView 3	79˚54'30.5496'' N 86˚00'38.7151'' W	3 (Pan-sharpened R, G, B)
Ellesmere Island 3 (EL3)	Slidre Fjord North 14, 08/09/2014	WorldView 2	79˚57'01.8072'' N 86˚10'18.5485'' W	3 (Pan-sharpened R, G, B)
Axel Heiberg 1 (AH1)	Axel Heibgerg 15, 29/07/2015	WorldView 3	79˚05'28.4936'' N 87˚00'09.0523'' W	3 (Pan-sharpened R, G, B)

Table 2. Summary of the delineation results for each method at each sample area and corresponding proportion of ice wedge volume

Sample area	Delineation method	Number of polygons (before edits)	Length of troughs (m)	Mean perimeter of polygons (m)	Mean area of polygons (m²)	Ice wedge volume (m³)	Frozen material volume (m³)	Proportion ice wedge volume (%)
EL1	Manual	164	6,220.44	62.11	255.53	12,753.25	280,401.53	4.55
	Thiessen Polygons	164	6,102.12	62.45	260.82	12,761.37	285,602.20	4.47
	Watershed Segmentation	164 (301)	6,105.08	61.28	256.26	12,541.60	280,611.55	4.47
EL2	Manual	56	3,457.68	100.67	624.60	6,905.93	224,451.24	3.08
	Thiessen Polygons	58	3,633.08	103.77	697.06	7,338.30	257,783.45	2.85
	Watershed Segmentation	56 (102)	3,399.87	101.58	627.63	6,829.92	221,567.01	3.08
EL3	Manual	271	7,896.53	47.82	149.04	16,515.05	280,986.34	5.88
	Thiessen Polygons	272	7,609.46	48.39	155.67	16,656.66	292,964.54	5.69
	Watershed Segmentation	271 (485)	7,942.68	48.24	149.49	16,580.42	281,982.11	5.88
AH1	Manual	9	1,568.67	243.48	2,709.50	2,603.85	150,828.45	1.73
	Thiessen Polygons	9	1,982.28	214.95	3,130.34	2,318.27	163,902.67	1.41
	Watershed Segmentation	9 (48)	1,417.94	211.27	2,692.54	2,280.17	148,990.71	1.53

Figures
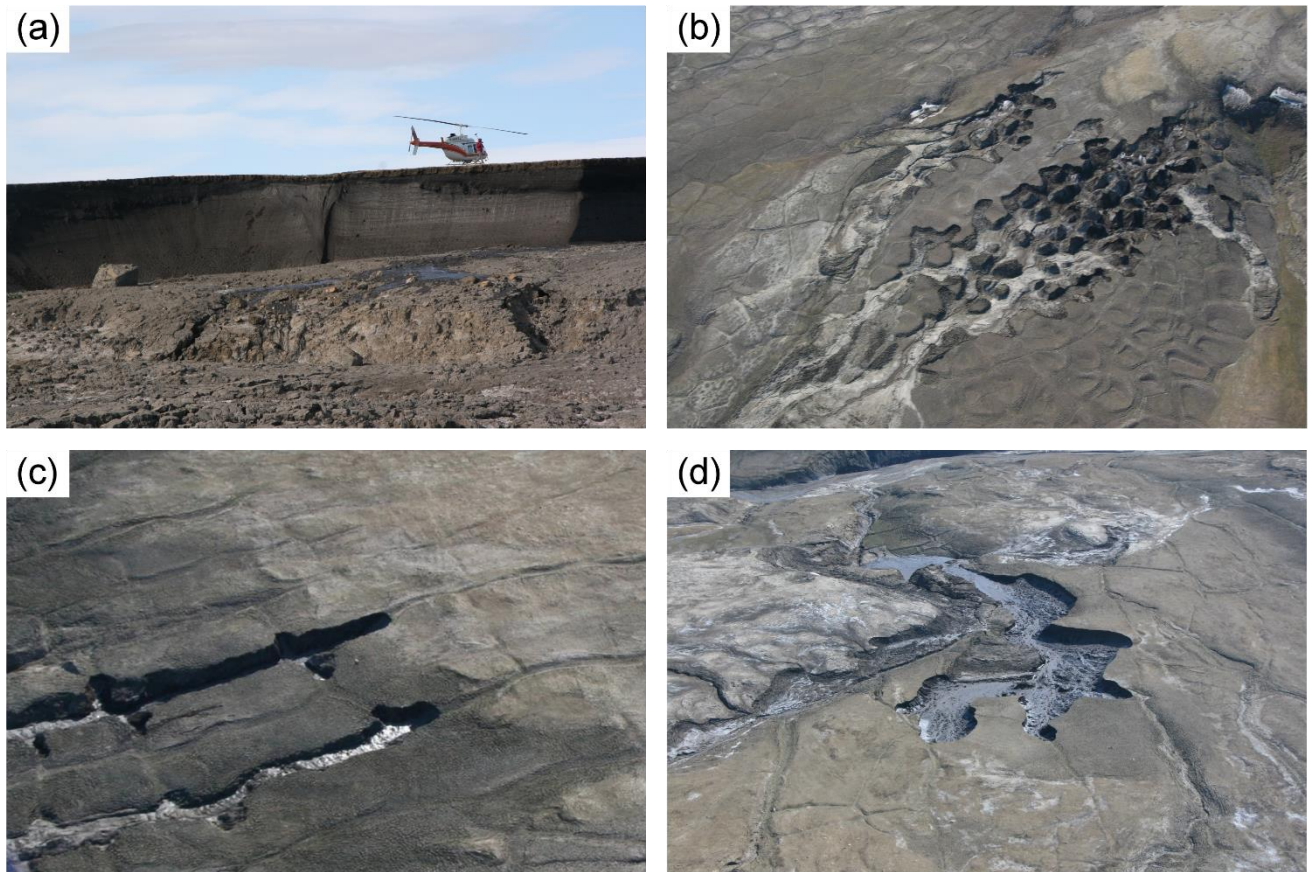
Figure 1. Thermokarst processes in the Eureka Sound Lowlands. (a) Retrogressive thaw slump headwall with an exposed ice wedge (~6 m depth) with no surface expression, Axel Heiberg Island, July 2016. Helicopter and person for scale. (b) Aerial view of an active melt out along ice wedge troughs and the resultant dissected landscape, Fosheim Peninsula, July 2015. (c) Example of back wasting of ice wedges melting out, Fosheim Peninsula. July 2013. (d) Rapid melt out of ice wedges where massive ice is present, Fosheim Peninsula July 2017.
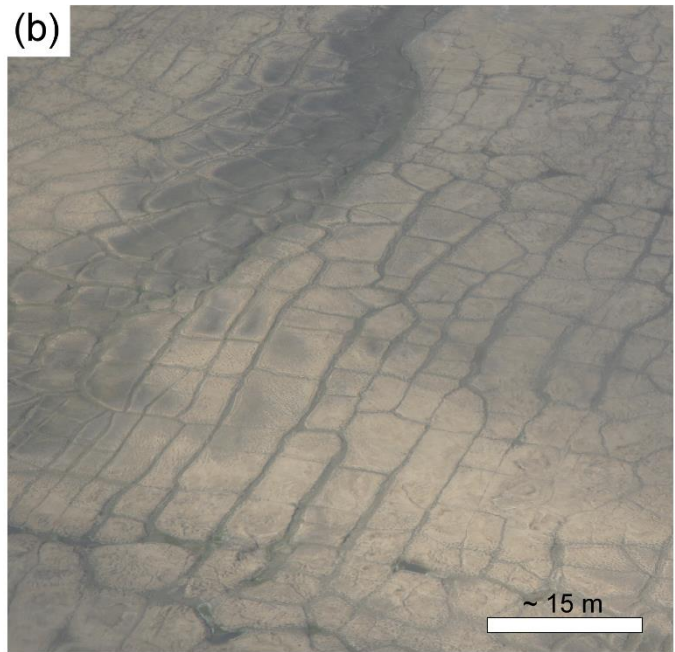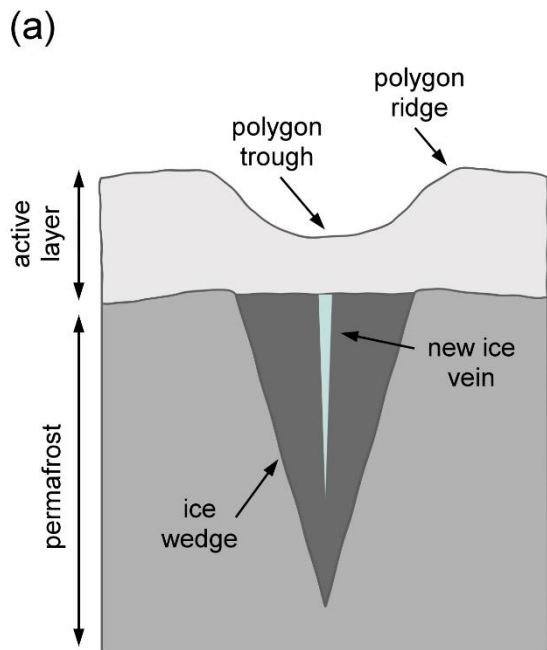
Figure 2. Ice wedges surface expression. (a) Representation of an epigenetic ice wedge in a high-centered polygon environment. **(b)** Aerial view of ice wedge polygons on the Fosheim Peninsula, Ellesmere Island.
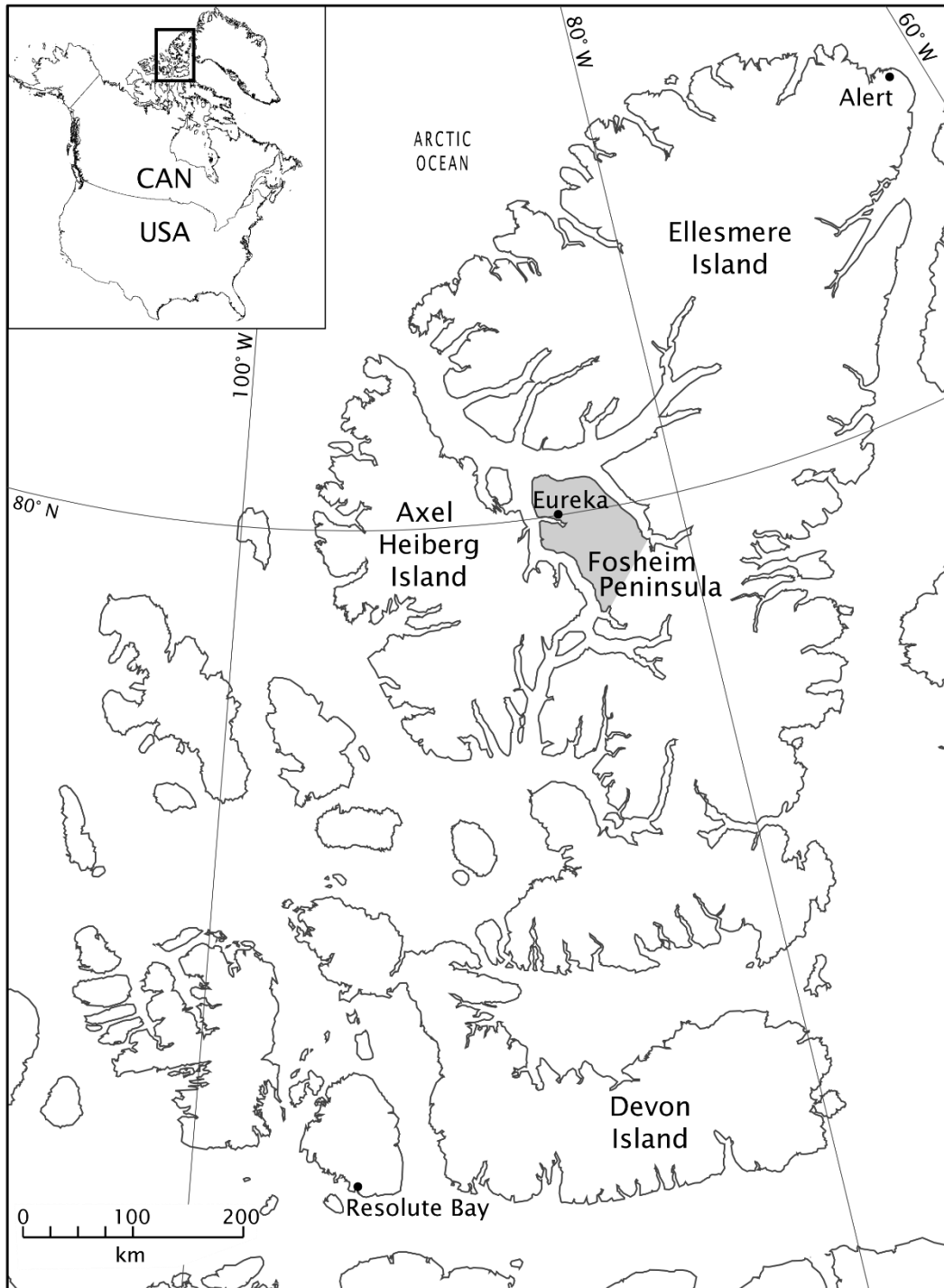
Figure 3. Location of the Fosheim Peninsula in the Canadian High Arctic.
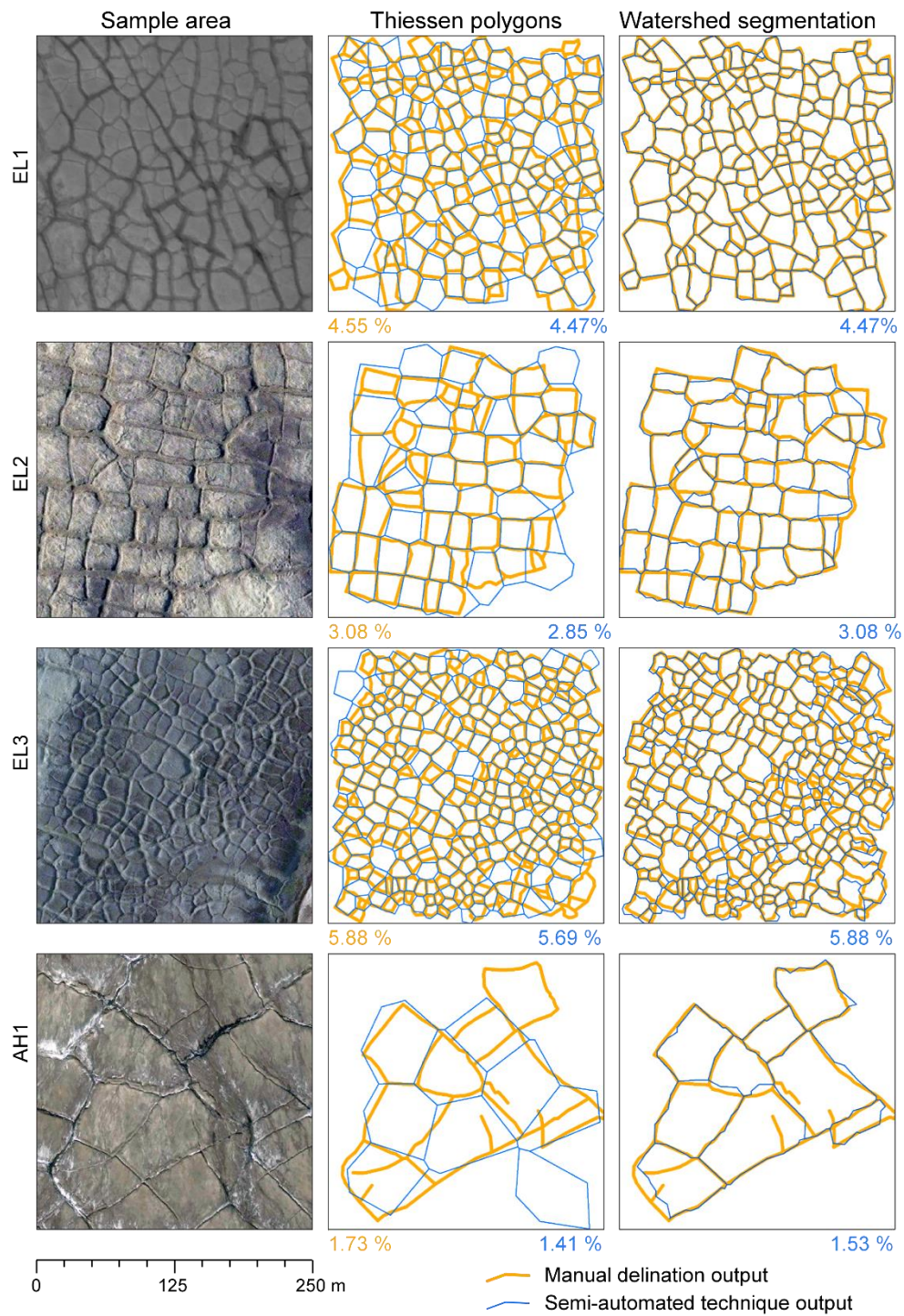
Figure 4. Original satellite image and delineation outputs with percentage of ice wedge volume in the top 5.9 m of permafrost for each method for each sample area.
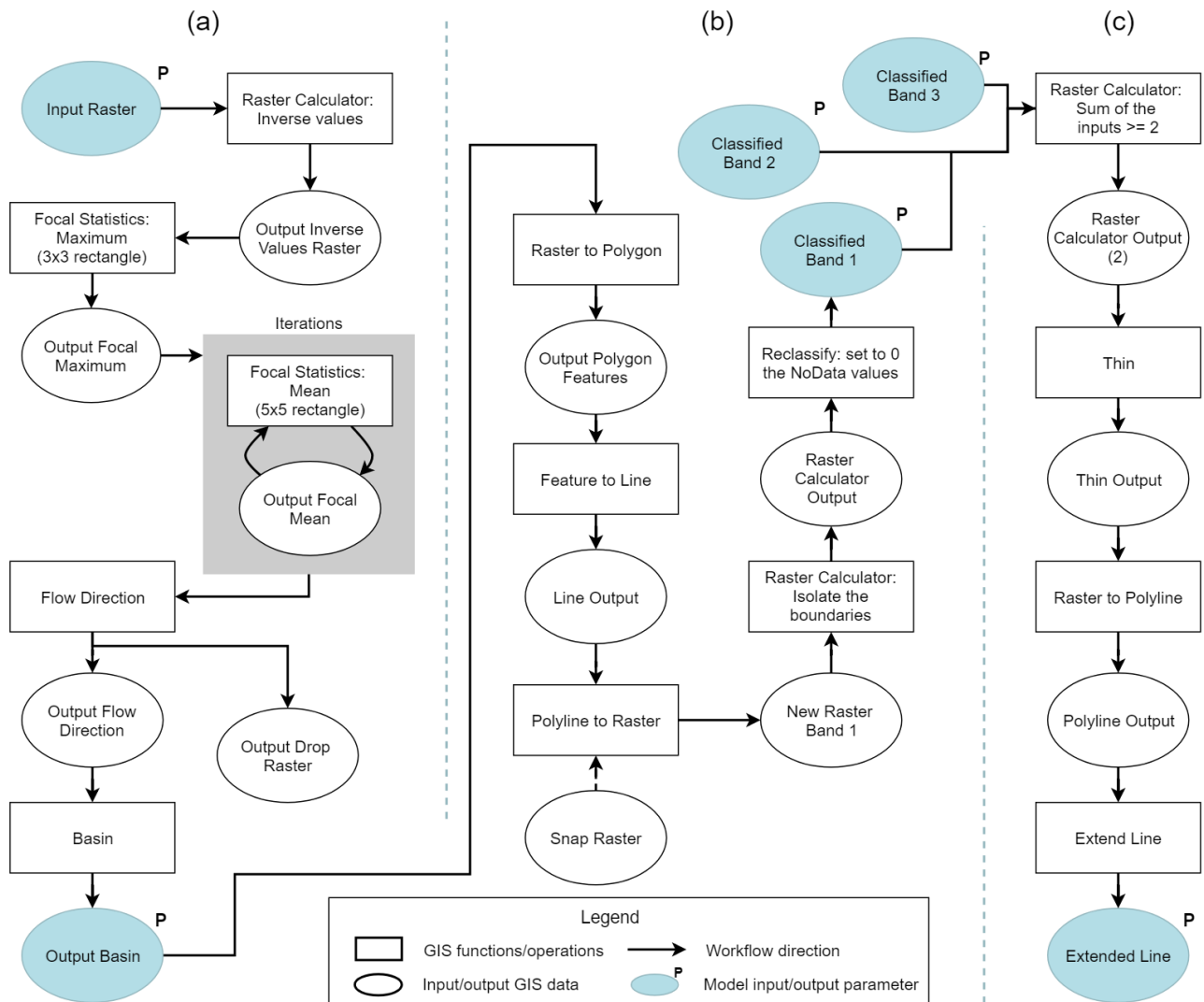
Figure 5. Models developed with ArcGIS Model Builder for the Watershed Segmentation method. (a) Watershed creation: the inputs are the raster image as well as its maximum and minimum values needed to inverse the pixel values. Treatment of each site differed in the number of iteration the Focal Statistic Mean tool had to be performed for a satisfying basin segmentation output. The output is a basin raster, where every pixel has the value of its corresponding watershed. **(b)** Converting Basin output to a raster of the watershed borders: watershed boundaries are classified as a raster where the value of 1 represent boundaries. The snap raster is the initial band image clipped to the sample area. **(c)** Combination of the bands: all the classified watershed boundaries of each band are converted to a line feature that can be manually edited. Detailed description of the tools can be found at http://desktop.arcgis.com/en/arcmap/10.3/main/tools/a-quick-tour-of-geoprocessing-tool-references.htm
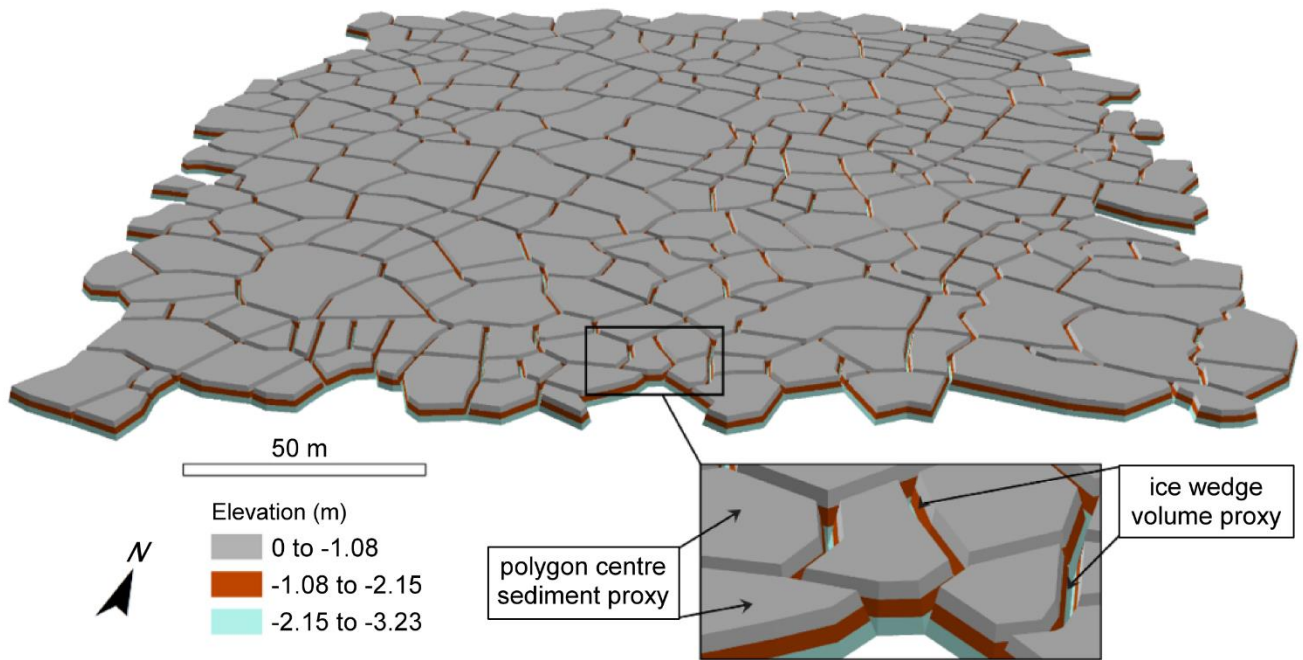
Figure 6. Example of a 3D subsurface model. The TIN surface represents the entire EL3 sample area (250 m x 250 m). The origin elevation is at the bottom of the active layer. This model is based on the methodology developed in Ulrich et al. (2014).
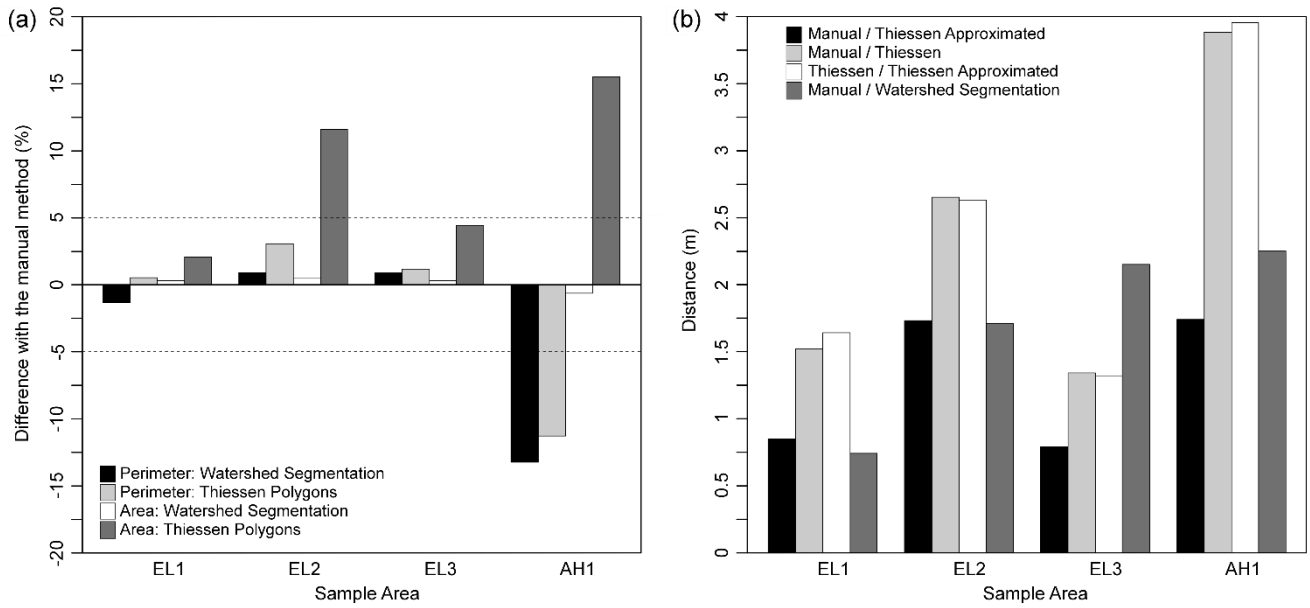
Figure 7. Delineation method comparison metrics. (a) Difference in mean area and perimeter of delineated polygons for the semi-automated methods with the manual delineation method. Refer to Table S1 for original data. (b) Mean distance between the centres of polygons created by the semi-automated delineation methods compared to the manual delineation method. The "Near" tool with a search radius of 10 m (20 pixels) was used. Two sets of centre points were considered for the Thiessen polygons method: the approximated centre point to create the polygons initially and the resulting centre points of the created Thiessen polygons. Refer to Table S2 for original data.
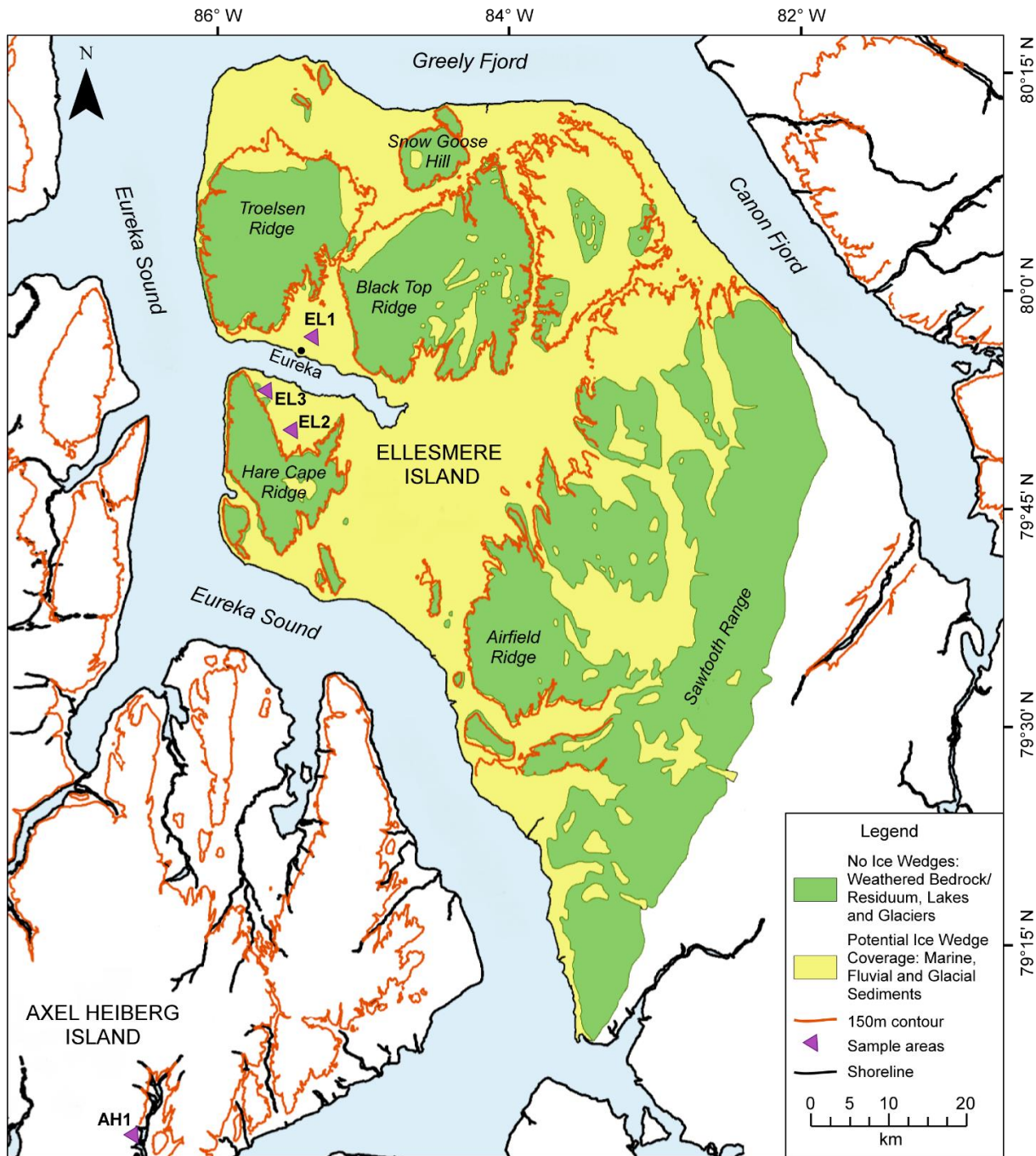
Figure 8. Potential coverage area of ice wedges on the Fosheim Peninsula. Based on the surficial geology map produced by Bell (1992). The contours (CanVec data, Natural Resources Canada, 2016) are a proxy for the Holocene sea level on the Peninsula (Bell, 1996). Coordinate System: NAD 1983 UTM 16N. Projection: Transverse Mercator.